Published in final edited form as:
Circulation. 2008 June 3; 117(22): 2919–2927. doi:10.1161/CIRCULATIONAHA.107.754614.

The Contribution of Macromolecular Structure to the Retention of LDL at Arterial Branch Points

Gina P. Kwon, BS[1], **Jamie L. Schroeder, BS**[1], **Marcelo J. Amar, MD**[2], **Alan T. Remaley, MD, PhD**[2], and **Robert S. Balaban, PhD**[1]

1 *Department of Health and Human Services, NIH, National Heart Lung and Blood Institute, Laboratory of Cardiac Energetics*

2 *Department of Health and Human Services, NIH, National Heart Lung and Blood Institute, Vascular Medicine Branch*

Abstract

Background—Extracellular deposition of low-density lipoproteins (LDL) in the arterial wall is an essential early step in atherosclerosis. This process preferentially occurs at arterial branch points, reflecting a regional variation in lipoprotein-arterial wall interactions. In this study, we characterized the sub-micron microstructure of arterial wall collagen and elastin to evaluate its potential role in regional LDL deposition.

Methods and Results—Using two-photon microscopy, the intrinsic optical properties of collagen and elastin were utilized to determine the arterial wall macromolecular microstructure in fresh porcine and murine arteries. This optical approach generated unique non-destructive *en face* three-dimensional views of the wall. The collagen/elastin microstructure was found to vary with the topology of the arterial bed. A nearly confluent elastin surface layer was present throughout, but was missing at atherosclerosis-susceptible branch points, exposing dense collagen-proteoglycan complexes. In LDL binding studies, this luminal elastin layer limited LDL penetration while its absence at the branches resulted in extensive LDL binding. Furthermore, LDL co-localized with proteoglycans with a sigmoidal dose dependence (inflection point ~130 mg LDL/dL). Ionic strength and competing anions studies were consistent with the initial interaction of LDL with proteoglycans to be electrostatic in nature.

Conclusions—This optical sectioning approach provided a robust three-dimensional collagen/elastin microstructure of the arterial wall in fresh samples. At atherosclerosis-susceptible vascular branch points, the absence of a luminal elastin barrier and presence of a dense collagen/proteoglycan matrix contributes to increased retention of LDL.

Keywords

atherosclerosis; aorta; coronary vessels; carotid; 2-photon excitation microscopy

Arterial wall mechanical properties and susceptibility to pathologic vascular remodeling, such as atherosclerosis, are determined by the macromolecular structure of collagen, elastin, and proteoglycans[1;2 3]. At low pressures, the high compliance of elastin dominates the wall displacement. At higher pressures, displacement is limited by the stiffer collagen. Changes in these mechanical properties with aging,[4] smoking,[5] diabetes,[6] hypertension,[7] and

Correspondence: Dr. Robert S. Balaban, National Institutes of Health, Bldg 10, Room B1D416, , Bethesda, MD 20892. E-mail E-mail: rsb@nih.gov. Fax (301) 402-2389. Phone (301) 496-2116.

Disclosures The authors have nothing to disclose with regard to this manuscript.

atherosclerosis [38]} are associated with modifications of the collagen and elastin scaffold. Although these macromolecules generate the wall's biphasic mechanical response to pressure, the specific nature of their microstructure remains an important missing element in the modeling of wall mechanics.[9, 10]

In addition to its influence on mechanical properties, the extracellular matrix plays an essential role in LDL accumulation in atherogenesis. Extracellular deposition of LDL in the arterial intima and media is an essential early step in this process.[11] In both humans[12] and animals,[13, 14] atherosclerosis develops preferentially at arterial branch points and certain regions of the aortic arch, including aortic branch points. The most popular hypothesis addressing this heterogeneity is that the distribution of low wall shear-stress and turbulence determines susceptibility.[15, 16] However, the absolute magnitude of wall stress and turbulence alone are inadequate to fully explain this heterogeneity since both mice and men have similar atherogenic regions with much different flow characteristics[17, 18]. Ahnother non-exclusive hypothesis for LDL accumulation involves the direct interaction of macromolecules with LDL. The Internal Elastic Lamina (IEL) serves as the major permeability barrier to water[19] as well as LDL[20] and limits LDL access to the wall while direct binding of LDL by collagen and proteoglycans is important in LDL retention.[21–23] Thus, the presence of the IEL along with collagen/proteoglycan content may be important factors in determining susceptibility. In this study we used two-photon microscopy and lumen-to-intima registered, *en face* optical sectioning through the intima and media to evaluate the distribution and structure of arterial wall macromolecules and their potential contribution to regional LDL retention.

Methods

Selection of tissue for imaging

We attempted to characterize three arterial beds in this study, the coronary, carotid and aorta. We selected the porcine coronary and carotid since these were of the appropriate size for this optical approach. The porcine aorta was too thick to permit transmural examinations as well as to large to screen different regions, thus the murine aorta was used as a substitute.

Mouse aorta preparation

Aorta samples were harvested from 20–28 week-old female C57BL/6J mice. Blood was removed by perfusion of the left ventricle of the heart with 1x Phosphate Buffer Solution (PBS) without calcium and magnesium (2.6 mM KCl, 1.4 mM KH_2PO_4, 136.8 mM NaCl, 8 mM Na_2HPO_4•$7H_2O$) (Quality Biological, Inc., Gaithersburg, MD). The aorta was dissected from the origin of the heart to the ileal bifurcation, cut longitudinally, and carefully placed endothelial cell surface down on the cover slip. A glass cover glass was secured to the covers slip with surgical tape on all four sides and the sample was immediately moved to the microscope for study. Samples were placed longitudinally across the stage and oriented in the same direction throughout the study. All experiments performed on animals were performed according to a research protocol (H-0050) approved by the Animal Care and Use Committee of the NHLBI, NIH.

Porcine coronary artery and carotid artery preparation

Pig hearts were harvested from anesthetized and heparinized (10,000 units i.v.) animals. Pig left carotid arteries were dissected and collected after the hearts were harvested and placed in Normal Saline (154mM NaCl) (Quality Biological, Inc., Gaithersburg, MD). The isolated heart was retrogradely perfused via the aorta with 500 mL cold buffer C (0.28 M sucrose, 10 mM N-2-hydroxyethylpiperazine-N′-2-ethanesulfonic acid (HEPES), and 0.2 mM EDTA, pH 7.21) to remove blood. The coronary arteries were isolated from the heart and immediately placed in normal saline. A 1 cm portion of the coronary artery was dissected from its aortic origin and

cut longitudinally. After extra fat and myocardial tissue were trimmed off of the artery, the vessel was placed luminal side down on a microscope cover and was covered by a glass slide. A 1 cm piece of the left carotid artery was also cut open longitudinally and placed luminal side down on a microscope cover and covered by a glass slide. The cover glass was loosely secured to the slide with surgical tape on all four sides and immediately moved to the microscope for study. Samples were placed longitudinally across the stage and oriented in the same direction throughout the study. All procedures performed were in accordance with the guidelines listed in the Animal Care and Welfare Act (7 U.S.C. 2142 § 13).

Two-photon excitation microscopy

All images were taken from the beginning of the intimal surface, through to the deeper medial layers. Two-photon images were taken at room temperature using a LSM 510 META microscope (Zeiss) with a 40X, 1.3 N.A. oil-immersion objective (Zeiss). Pig coronary arterial images taken for the purpose of measuring relative LDL binding concentrations were taken with a 40X, 1.2 N.A. water objective (Zeiss). A pulsed Ti:Sapphire laser (Coherent) set at 860 nm was used for excitation, unless a different frequency is noted. Emitted light from the sample was passed through an IR-blocking BG39 filter, a spectral dispersion grating resident in the Zeiss META system, and was detected by an array of PMTs generating a 10.7 nm spectral resolution. Emission spectra were collected to optimize the separation of collagen and elastin signals[24]. Emission spectra (Figure S1) reveals that below 840 nm excitation the near UV second harmonic generation (SHG) signal was suppressed, likely because of the transmission characteristics of the optics as well as the inner filter properties of the tissues.[25] Thus, an excitation above 840 nm (i.e. 420nm single photon) was required to detect the collagen SHG. The elastin fluorescence emission was found to shift with excitation frequency (Ef), suggesting multiple chromophores within elastin. The insert in Figure S1 shows a plot of the difference in peak frequency of elastin fluorescence versus the collagen SHG as a function of Ef. The spectral difference between elastin and collagen decreased with increasing Ef. Thus, the lower the Ef, the better the separation of the collagen and elastin signals. With the lower end of the detection of the second harmonic at 840 nm, we selected an Ef of 860 nm for these studies. Elastin fluorescence was measured from 500–533 nm, while collagen SHG was measured from 393–436 nm. The collagen signal was completely excluded from the elastin channel, and the contamination of elastin in the collagen channel was < 2%.

LDL was labeled with Alexa Fluor-647 and images of the pig coronary were acquired with dichroic mirrors and bandpass filters. Collagen SHG was detected at 415–430nm, elastin fluorescence at 500–550 nm and AlexaFluor-647 (LDL) at 650–710nm.

Three-dimensional images were generally collected as a stack of images at 1 μm spacing starting at the luminal surface of the vessel. For qualitative studies, the gain and laser power was generally increased with increasing depth into the tissue to optimize the signal to noise ratio. More specific imaging parameters for each figure image may be found in the supplementary methods section.

Relative quantification of collagen SHG signal in the mouse aortic intima-media

Using two-photon microscopy, quantification of relative superficial collagen content within atherosclerosis-prone aortic arch branch points and resistant areas in the murine aortic wall was accomplished by measuring the collagen SHG signal/volume from the luminal surface to the beginning of the collagen-rich adventitia. Four to five images were acquired in each region in five mouse aortas and averaged for analysis. The backscattered SHG pixel intensity was integrated from the surface to 15–20 μm deep. Normalization was performed by dividing the SHG signal integrals by the measurement volume to correct for overall wall thickness. The calculated SHG pixel densities were then squared to get the relative collagen content.

To determine the amplitude of the orientation effect collagen fibrils within different parts of the aortic wall, the SHG signal of twenty random locations in the murine lower abdominal aortic wall were quantified by integrating the entire SHG signal, in paired studies, from the surface to 20–30 μm deep with the fibrils grossly arranged parallel to the laser then rotating the sample 90°. The 90° rotation resulted in only a ~6% ($p = 0.01$) increase in calculated collagen content. For further discussion, please see the Extended Methods section online.

LDL preparation

LDL was isolated from 250 ml of blood freshly collected from donor human plasma by sequential ultracentrifugation (4 °C, 100,000 rpm for 5 h) after density adjustment with KBr (d = 1.019–1.063 g/ml), using a TLA-100.2 rotor on a Beckman tabletop ultracentrifuge (Beckman Instruments, Palo Alto, CA). After extensive dialysis against phosphate-buffered saline containing EDTA and sodium azide, particle integrity was confirmed by native agarose gel. LDL concentration was estimated by measuring total protein concentration. LDL was labeled with Alexa Fluor-647 protein labeling kit (Molecular Probes, Eugene, OR) which has a succinimidyl ester moiety that reacts with primary amines of proteins to form stable dye-protein conjugates. At the last step of the labeling process, labeled LDL was eluted from the separation column using PBS with 2mM azide provided in the kit or was eluted with Normal Saline, dH_2O or buffer B (120 mM NaCl, 3 mM KCl, 2 mM $CaCl_2$, 1 mM MgCl2, 1 mM KPO4, and 2 mM HEPES). LDL was concentrated using a centrifugal filter device with a nominal molecular weight limit of 10 kDa (Millipore, Billerica, MA).

LDL binding studies

The endothelial cell layer was denuded from 1 cm segments of pig coronary arteries by gentle scraping with a cell scraper. Coronary segments were incubated in 1.5 mL eppendorf tubes at room temperature with various concentrations of labeled-LDL prepared in the appropriate buffer. They were then washed in a matching buffer solution for one hour to remove any free dye. Steady state binding studies at branch points were done in PBS with a 2:1 ratio of unlabeled LDL to Alexa Fluor labeled LDL. Experiments done in bicarbonate buffer B had 25 mM $NaHCO_3$ added immediately prior to incubation and the incubation was done in a 5% CO_2 incubator at 37°C with the sample tube open.

Relative LDL signal per volume was measured using two-photon microscopy by integrating the LDL pixel intensity from the luminal surface to the point in the wall where its signal had nearly disappeared (approximately 15–30 μm). Normalization was performed by dividing the LDL signal integral by the measurement volume.

Proteoglycan labeling

For labeling proteoglycan distribution anti-heparan antibody (Seikagaku Corporation, East Falmouth, MA) was labeled with an Alexa Fluor-564 antibody labeling kit (Molecular Probes, Eugene, OR). The endothelial cell layer was denuded from 1 cm segments of pig coronary artery by gentle scraping with a cell scraper. Coronary segments were blocked with 5% Bovine Serum Albumin (BSA) in buffer B at room temperature for 1 hour. Alexa Fluor-564 labeled heparan antibody was diluted (1:50) in a 5% BSA solution and arterial samples were incubated with the antibody at room temperature for 1 hour at room temperature and then at 4°C overnight. Samples were washed with buffer B for 30 min. and subsequently incubated with LDL in physiologic ionic conditions as stated above.

Colocalization analysis of LDL with collagen or proteoglycans

The first 20 slices of the z-series images were analyzed for LDL colocalization with collagen. The first 2–3 slices of the z-series images were analyzed for LDL colocalization with surface

proteoglycans. Quantification of colocalization was carried out using Imaris 5.7 software package (Bitplane AG, Zurich, Switzerland). Pixel codistribution was calculated for the false colored blue collagen or false colored green proteoglycan with false colored red LDL throughout the three dimensional data sets. Approximately 20% of the field of view was reduced into a region of interest (ROI) for analysis selected by the collagen or proteoglycan distribution. The colocalized pixels (voxels in 3D) were displayed in a white mask overlapping the fluorescence channels. Two-dimensional histograms (fluorograms) show the distribution of pixel intensities. The percentage of colocalized material (intensity and volume) was analyzed and Pearson correlation coefficients in the ROI (R_{coloc}; 1 = perfect correlation, 0 = no correlation, and −1 = perfect inverse correlation) were compared.

Imaging LDL Binding to Mouse Aortas

Wide field of view images of the mouse aorta were obtained with an OV110 Small Animal Imaging System (Olympus). Four parfocal and parcentered objectives provide a zoom range of several orders of magnitude (0.1x to 16x) with high numerical aperture (0.43–0.07). A xenon bulb with bandpass excitation filter of 610–645 nm (Olympus) was used as a light source and fluorescence was measured with a high sensitivity CCD camera (Hamamatsu) filtered by a 675–715 nm bandpass emission filter (Olympus). 512 x 512 x 8 images were obtained using a 0.89X/0.04 N.A. objective. For higher magnification objectives (>1x) a dichroic mirror reflecting below 665 nm was used, while with lower magnification objectives, no dichroic was used and excitation and emission followed separate beam paths. Images were automatically optimized for brightness and contrast with a linear LUT.

Statistical analysis

All data are expressed as means ± standard deviation. Wilcoxon rank sum test was performed to analyze the differences of collagen content between the aortic arch and the abdominal aortic. Statistically significant differences of collagen content between the parallel and perpendicular sample orientation were assessed by two-tailed Student's t-test since the orientation of the collagen fibrils was not uniformly aligned to the laser polarization[26]. The sigmoid binding curve obtained from steady state binding studies of LDL was fitted and a three parameter equation was derived using SigmaPlot 8.0.

The authors had full access to and take full responsibility for the integrity of the data. All authors have read and agree to the manuscript as written.

Results

Mouse Aorta

The collagen and elastin microstructure was determined for various regions in the C57BL/6J mouse aorta (n = 6). Along the free wall of the thoracic aorta, elastin formed lamellar layers (Figure 1A). The most superficial layer was a continuous sheet covering the luminal surface. With no intra-luminal pressure, the arterial wall surface compressed in the radial direction into longitudinal wavy folds reflecting the residual circumferential stress, or "residual strain," within the intima-medial layers. The "wavy" nature of these folds indicated that both radial and longitudinal residual strain was occurring. The spacing of the lamellar folds was approximately 50–100 μm in the upper thoracic aorta and 30–50 μm in the lower abdominal aorta. Coiled collagen fibers were radially arranged within the compressed inner folds of the elastin lamellae as well as between each lamellar unit (Figure 1A and 1B). Individual collagen fibers were coiled with a mean periodicity of 2–5 μm (Figure 1B). Moving out to the adventitia, the abundant Second Harmonic Generation (SHG) signal from tortuous collagen fibers overwhelmed the image. At atherosclerosis-prone intervertebral branch points, collagen fibrils were circumferentially organized in a knotted ring surrounding the ostia (Figure 1C). Unlike

in the free wall, the ostia were mostly uncovered by an elastin layer. Further from the ostia, the insertion of the branch deflected parallel collagen fibers, generating denser collagen structures. These collagen fibers did not show sinusoidal compression, suggesting minimal residual stress at branch regions consistent with the high collagen content. Similarly, collagen at aortic arch branch points formed dense knotted structures (Figure 1D). Relative quantification of superficial collagen content with two-photon microscopy showed the mean collagen density in the aortic arch to be 53.8 ± 5.6 (s.d.) Arb Unit/μm^3, and the mean collagen density in the abdominal aortic wall to be 41.0 ± 3.6 (s.d.) Arb Unit/μm^3 in 5 paired experiments. There was a 24% higher density of collagen in the aortic arch branch regions than the free abdominal wall (P=0.05, Wilcoxon rank sum test).

Porcine Carotid Artery

Similar elastin and collagen microstructure was seen in the porcine carotid artery as in the mouse distal aorta. The porcine carotid artery had a superficial layer of elastin covering the luminal surface (n = 6) (Figure 2). This layer was compressed in the radial direction into longitudinal wavy folds spaced approximately 40–80 μm apart. In contrast to the murine aorta, the surface elastin in the porcine carotid artery had larger circular openings throughout. There was approximately 0.002–0.004 openings per μm^2 and each opening ranged in size from small circular holes that were 3 μm in diameter to larger oval holes that were 25 μm by 9 μm in size. Similar to the murine aorta, collagen fibers in the porcine carotid artery were radially arranged within the inner folds of the elastin layer and were coiled with a mean periodicity of 5–10 μm.

Porcine Coronary Artery

Macromolecular images of the porcine coronary artery were collected from the free wall and branch points (n = 6). In the free coronary arterial wall the elastin was limited to the single IEL layer in contrast to the porcine carotid artery and the murine aorta (Figure 3A). The IEL was fenestrated, with individual elastin fibers arranged into a net-like structure over the luminal surface. The residual strain resulted in longitudinal folds with spacing of 30–50 μm, implying a dominant radial stress. Collagen associated with the surface of the IEL was amorphous and ran roughly parallel with the longitudinal elastin fibers. Beneath the IEL, collagen fibrils were radially arranged throughout the tunica media, with few elastic fibrils intermixed between collagen fibers. The fact that the elastin fibers of the IEL and its folds were parallel indicated that the deeper layers running perpendicular to the IEL fibers dominated the residual strain. A close examination of a coronary artery branch point is presented in Figure 3B, 3C and 3D. Serial images taken through coronary branch points were taken from the free wall (Figure 3B), through the annulus (Figure 3C), the edge of the cut branch artery (Figure 3D) The IEL thinned and ended at the annulus exposing a dense mesh of collagen and its associated proteoglycans. This branch point structure was qualitatively similar to the branch point structures observed in the mouse aorta (Figure 1C) where the surface elastin layer was absent at the branch point ostia.

LDL Binding

LDL binding to specific ECM components was monitored in arterial samples using 4 mg/mL of fluorescently labeled LDL in physiological buffer B in the absence of convective flow. By performing these studies *in vitro* with no flow, the physical contribution of flow and pressure gradients in LDL binding distribution was eliminated. The endothelial cell layer was removed for these studies to eliminate the potential contribution of localized endothelial cell damage during preparation to influence the binding assay. LDL bound most abundantly within the exposed collagen at porcine coronary arterial branches (Figure 4A) but not in the free wall where the elastin layer apparently restricted the penetration of LDL (Figure 4B) (n = 6). Similarly, wide field single photon excitation fluorescence imaging of the murine aorta showed

extensive LDL binding within the structures surrounding the intervertebral branch points while LDL was excluded from the free wall of the aorta (Figure 5) (n = 3).

Based on these observations, we focused on the characterization of LDL binding to the porcine coronary branch points. Wash-out studies showed a complete wash-out of free AlexaFluor from branch points after one hour, while the AlexaFluor labeled LDL was unaffected by extensive washing consistent with a very tight association of LDL with the macromolecules (Figure S2). It has previously been reported that the association of LDL to vascular wall macromolecules is an electrostatic interaction.[27] We found that low ionic strength media, such as water, significantly increased LDL binding (Figure 6A) over normal saline (Figure 6B). In contrast, the addition of competing anions such as 2 mM azide to PBS almost completely blocked LDL binding (Figure 6C). These results are consistent with the notion that LDL binding is electrostatic in nature, increasing with decreasing ionic strength and is in competition with multivalent anions.

The steady state kinetics of LDL binding at coronary branch points was determined by varying LDL concentration in the bath. Time courses revealed a plateau at near 100 min. (Figure 4C). Thus 120 min. incubation times were used for the LDL binding experiments. The steady state binding kinetics of LDL revealed a sigmoid binding curve with an inflection point near 130 mg LDL/dL suggesting a cooperative binding mechanism (Figure 4D).

Co-localization analysis in the coronary branch point revealed very little correlation between LDL and collagen (n = 3, $R_{coloc} = 0.056 \pm 0.075$) (Figure 7A). In contrast, the degree of co-localization between LDL and immune-labeled proteoglycans was relatively high (n = 3, $R_{coloc} = 0.469 \pm 0.030$) (Figure 7B and 7C). The correlation of LDL and proteoglycans was not perfect and inspection of the images suggested that only a sub-set of the labeled proteoglycans were interacting with LDL. This is consistent with the nature of the antibody used that is rather non-specific for the different proteoglycan sub-types.

Discussion

These data provide the three-dimensional microstructure of arterial wall collagen and elastin in different arterial beds. This information is useful for the quantitative modeling of arterial wall mechanics as well as the analysis of water and macromolecular permeability. The non-destructive optical sectioning methods presented here should aid in the future characterization of pathological vascular remodeling by providing fully registered, high resolution 3D images of the vascular microstructure.

A major difference among various arterial beds was the structure of the surface elastin layer, a barrier that is believed to play a key role in the water and LDL permeability.[19, 20] Structural differences in elastin are highlighted by observing three different arterial structures from the pig. A surface rendering of the surface elastin layer in the porcine aorta, carotid, and coronary vessels is presented in Figure 8. Despite the large thickness of the porcine aorta, a good examination of the surface elastin can be made with this optical approach. In contrast to the nearly confluent murine aorta elastin layer, the porcine aorta elastin layer was clearly non-confluent and revealed a significant amount the underlying collagen. The large differences in macromolecular structure in the porcine and murine aorta suggest that species differences need to be considered in extrapolating these data. On a macroscopic view, the predicted relative permeability would be highest in the porcine aorta, then in the coronary and carotid arteries. The predicted permeability of the aorta and coronary correlates well these structures' general susceptibility to lipid deposition in young men.[28] Another striking structural feature was the absence of this elastin barrier and the exposure of a dense collagen/proteoglycan network at arterial branch points in both the porcine and murine models. These alterations in

microstructure likely reflect the different mechanical stress encountered by these arterial branch points.[29] LDL preferentially bound within the proteoglycan structures of these branch points, consistent with the absence of the elastin barrier. The interaction in this dense collagen/proteoglycan network was consistent with an initial electrostatic interaction with proteoglycans followed by a hydrophobic self association of LDL resulting in the cooperative kinetics of binding (Figure 6D).[27, 30]

The two models of early LDL deposition in atherosclerosis involve low shear stress and turbulent flow characteristics[15, 16], influencing both transport and gene expression alterations, or macromolecule retention of LDL [11, 22, 23, 31] These two models are brought together by our observations since both low shear flow and modifications of macromolecular structure that promote LDL retention are occurring in the same atheroma-prone regions. It is possible that the macromolecular structure observed in this study is a direct result of molecular signaling associated with low shear stress. For example, Platt et al[32] demonstrated that laminar flow may protect the elastic lamina by inhibiting cathepsins, a potent stimulants of elastin breakdown, while others have demonstrated that low shear stress activate several other potential elastin proteases[33, 34]. These enzymatic alterations associated with low shear stress *in vitro*, could explain the compromise of the elastin layer at arterial branch points. However, other mechanical aspects of the vascular branch point may also be important in generating this macromolecular structure. Independent of the mechanism of generation, it is unclear what physiological role the removal of the surface elastin layer may play at these vascular branch points. In any event, the macromolecular structure of arterial branch points potentiates the retention of LDL along with many of the other documented physiological effects associated with low shear flow occurring in these regions.

It is of interest to attempt to correlate the steady state binding kinetics of LDL at coronary branch points with clinical risk factors and outcomes. First, the highly non-linear, cooperative nature of the binding is consistent with the notion that small changes in plasma concentration of LDL will result in large differences in binding and potential atherogenesis.[35] Notably, the inflection point of the LDL binding curve at around 130 mg/dL (Figure 4D) is near the LDL concentration at which the American Heart Association recommends starting medical therapy in patients with elevated lipids.[36] Although this value was determined from clinical outcomes, the association of LDL with vascular wall proteoglycans in this highly non-linear fashion may provide a molecular mechanism explaining the significance of this empirical value as an important risk factor in atherogenesis and the high sensitivity of clinical outcome to small alterations in plasma LDL levels.

Acknowledgments

The authors would like to acknowledge conversations concerning the angular dependence of the backscattered SHG signal with Dr. Paul Campagnola and helpful discussion with Dr. Chris Combs. We would also like to thank Dr. Daniela Malide for help with co-localization measurements as well as Dr. John Stonik for help with the LDL preparations.

Funding This work was supported by the intramural research division of the National Heart Lung and Blood Institute, NIH.

Reference List

1. Dobrin PB. Mechanical properties of arteries. Physiol Rev 1978;58:397–460. [PubMed: 347471]
2. Glasser SP, Arnett DK, McVeigh GE, Finkelstein SM, Bank AJ, Morgan DJ, Cohn JN. Vascular compliance and cardiovascular disease: a risk factor or a marker? Am J Hypertens 1997;10:1175–89. [PubMed: 9370391]
3. Ross R. The pathogenesis of atherosclerosis: a perspective for the 1990s. Nature 1993;362:801–9. [PubMed: 8479518]

4. Kelly R, Hayward C, Avolio A, O'Rourke M. Noninvasive determination of age-related changes in the human arterial pulse. Circulation 1989;80:1652–9. [PubMed: 2598428]
5. McVeigh GE, Morgan DJ, Finkelstein SM, Lemay LA, Cohn JN. Vascular abnormalities associated with long-term cigarette smoking identified by arterial waveform analysis. Am J Med 1997;102:227–31. [PubMed: 9217589]
6. Lehmann ED, Gosling RG, Sonksen PH. Arterial wall compliance in diabetes. Diabet Med 1992;9:114–9. [PubMed: 1563244]
7. Heagerty AM, Aalkjaer C, Bund SJ, Korsgaard N, Mulvany MJ. Small artery structure in hypertension. Dual processes of remodeling and growth. Hypertension 1993;21:391–7. [PubMed: 8458640]
8. Libby P, Theroux P. Pathophysiology of coronary artery disease. Circulation 2005;111:3481–8. [PubMed: 15983262]
9. Bank AJ, Wang H, Holte JE, Mullen K, Shammas R, Kubo SH. Contribution of collagen, elastin, and smooth muscle to in vivo human brachial artery wall stress and elastic modulus. Circulation 1996;94:3263–70. [PubMed: 8989139]
10. Pandit A, Lu X, Wang C, Kassab GS. Biaxial elastic material properties of porcine coronary media and adventitia. Am J Physiol Heart Circ Physiol 2005;288:H2581–H2587. [PubMed: 15792993]
11. Williams KJ, Tabas I. The response-to-retention hypothesis of early atherogenesis. Arterioscler Thromb Vasc Biol 1995;15:551–61. [PubMed: 7749869]
12. Velican D, Velican C. Study of fibrous plaques occurring in the coronary arteries of children. Atherosclerosis 1979;33:201–5. [PubMed: 475879]
13. Schwenke DC, Carew TE. Initiation of atherosclerotic lesions in cholesterol-fed rabbits. I. Focal increases in arterial LDL concentration precede development of fatty streak lesions. Arteriosclerosis 1989;9:895–907. [PubMed: 2590067]
14. Thubrikar MJ, Keller AC, Holloway PW, Nolan SP. Distribution of low density lipoprotein in the branch and non-branch regions of the aorta. Atherosclerosis 1992;97:1–9. [PubMed: 1445489]
15. Friedman MH, Deters OJ. Correlation among shear rate measures in vascular flows. J Biomech Eng 1987;109:25–6. [PubMed: 3560875]
16. Lei M, Kleinstreuer C, Truskey GA. Numerical investigation and prediction of atherogenic sites in branching arteries. J Biomech Eng 1995;117:350–7. [PubMed: 8618389]
17. Feintuch A, Ruengsakulrach P, Lin A, Zhang J, Zhou YQ, Bishop J, Davidson L, Courtman D, Foster FS, Steinman DA, Henkelman RM, Ethier CR. Hemodynamics in the mouse aortic arch as assessed by MRI, ultrasound, and numerical modeling. Am J Physiol Heart Circ Physiol 2007;292:H884–H892. [PubMed: 17012350]
18. Suo J, Ferrara DE, Sorescu D, Guldberg RE, Taylor WR, Giddens DP. Hemodynamic shear stresses in mouse aortas: implications for atherogenesis. Arterioscler Thromb Vasc Biol 2007;27:346–51. [PubMed: 17122449]
19. Jayaraman G. Water transport in the arterial wall--a theoretical study. J Biomech 1983;16:833–40. [PubMed: 6643521]
20. Tada S, Tarbell JM. Internal elastic lamina affects the distribution of macromolecules in the arterial wall: a computational study. Am J Physiol Heart Circ Physiol 2004;287:H905–H913. [PubMed: 15016628]
21. Boren J, Olin K, Lee I, Chait A, Wight TN, Innerarity TL. Identification of the principal proteoglycan-binding site in LDL. A single-point mutation in apo-B100 severely affects proteoglycan interaction without affecting LDL receptor binding. J Clin Invest 1998;101:2658–64. [PubMed: 9637699]
22. Jimi S, Sakata N, Matunaga A, Takebayashi S. Low density lipoproteins bind more to type I and III collagens by negative charge-dependent mechanisms than to type IV and V collagens. Atherosclerosis 1994;107:109–16. [PubMed: 7945553]
23. Khalil MF, Wagner WD, Goldberg IJ. Molecular interactions leading to lipoprotein retention and the initiation of atherosclerosis. Arterioscler Thromb Vasc Biol 2004;24:2211–8. [PubMed: 15472124]
24. Jobsis PD, Ashikaga H, Wen H, Rothstein EC, Horvath KA, McVeigh ER, Balaban RS. The visceral pericardium: macromolecular structure and contribution to passive mechanical properties of the left ventricle. Am J Physiol Heart Circ Physiol 2007;293:H3379–H3387. [PubMed: 17933976]
25. Rothstein EC, Nauman M, Chesnick S, Balaban RS. Multi-photon excitation microscopy in intact animals. J Microscopy 2006;222:58–64.

26. Williams RM, Zipfel WR, Webb WW. Interpreting second-harmonic generation images of collagen I fibrils. Biophys J 2005;88:1377–86. [PubMed: 15533922]
27. Camejo G, Lopez A, Lopez F, Quinones J. Interaction of low density lipoproteins with arterial proteoglycans. The role of charge and sialic acid content. Atherosclerosis 1985;55:93–105. [PubMed: 4004985]
28. Strong JP, Malcom GT, McMahan CA, Tracy RE, Newman WP III, Herderick EE, Cornhill JF. Prevalence and extent of atherosclerosis in adolescents and young adults: implications for prevention from the Pathobiological Determinants of Atherosclerosis in Youth Study. JAMA 1999;281:727–35. [PubMed: 10052443]
29. Thubrikar MJ, Robicsek F. Pressure-induced arterial wall stress and atherosclerosis. Ann Thorac Surg 1995;59:1594–603. [PubMed: 7771858]
30. Camejo G, Lalaguna F, Lopez F, Starosta R. Characterization and properties of a lipoprotein-complexing proteoglycan from human aorta. Atherosclerosis 1980;35:307–20. [PubMed: 7362702]
31. Chatzizisis YS, Coskun AU, Jonas M, Edelman ER, Feldman CL, Stone PH. Role of endothelial shear stress in the natural history of coronary atherosclerosis and vascular remodeling: molecular, cellular, and vascular behavior. J Am Coll Cardiol 2007;49:2379–93. [PubMed: 17599600]
32. Platt MO, Ankeny RF, Jo H. Laminar shear stress inhibits cathepsin L activity in endothelial cells. Arterioscler Thromb Vasc Biol 2006;26:1784–90. [PubMed: 16709945]
33. Magid R, Murphy TJ, Galis ZS. Expression of matrix metalloproteinase-9 in endothelial cells is differentially regulated by shear stress. Role of c-Myc. J Biol Chem 2003;278:32994–9. [PubMed: 12816956]
34. Bassiouny HS, Song RH, Hong XF, Singh A, Kocharyan H, Glagov S. Flow regulation of 72-kD collagenase IV (MMP-2) after experimental arterial injury. Circulation 1998;98:157–63. [PubMed: 9679722]
35. Cullen P, Schulte H, Assmann G. Smoking, lipoproteins and coronary heart disease risk. Data from the Munster Heart Study (PROCAM). Eur Heart J 1998;19:1632–41. [PubMed: 9857915]
36. Smith SC Jr, Blair SN, Bonow RO, Brass LM, Cerqueira MD, Dracup K, Fuster V, Gotto A, Grundy SM, Miller NH, Jacobs A, Jones D, Krauss RM, Mosca L, Ockene I, Pasternak RC, Pearson T, Pfeffer MA, Starke RD, Taubert KA. AHA/ACC Guidelines for Preventing Heart Attack and Death in Patients With Atherosclerotic Cardiovascular Disease: 2001 update. A statement for healthcare professionals from the American Heart Association and the American College of Cardiology. J Am Coll Cardiol 2001;38:1581–3. [PubMed: 11691544]

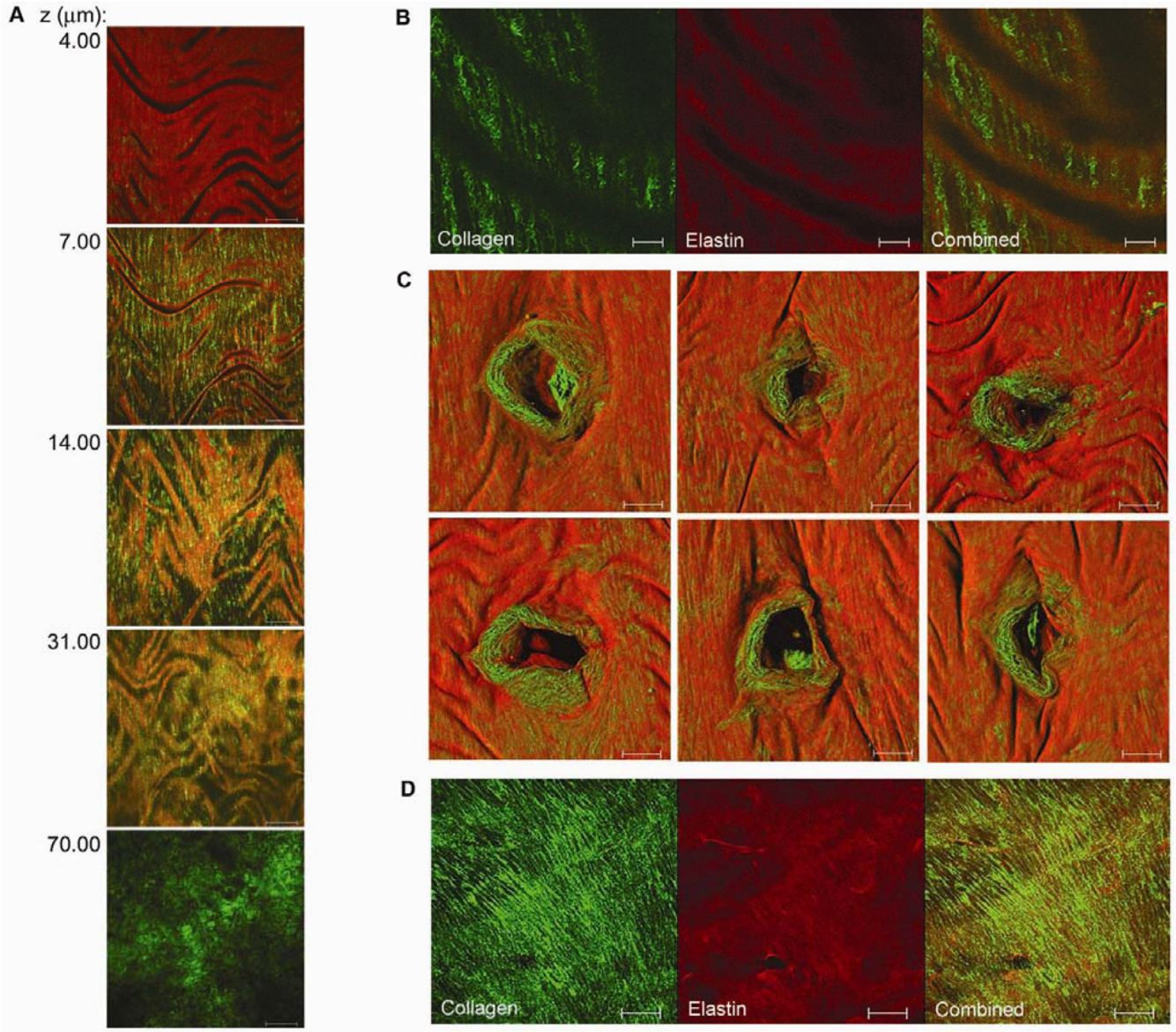

Figure 1.

Collagen and elastin microstructure of the mouse aorta. A, Two-photon z-series images through the thoracic aortic wall, starting from the luminal surface (4.00 μm) through to the adventitia (70.00 μm). Elastin auto-fluorescence is red and the collagen SHG is green. A nearly confluent, wavy sheet of elastin envelops the luminal surface of the aortic wall. Collagen fibrils are radially arranged within the inner folds of the elastin lamellae as well as between lamellar units. Further out from the lumen, tortuous collagen fibrils make up the adventitia. Scale bar, 50 μm. This series demonstrates that both the intima-media interface, classically marked by the internal elastic lamina, as well as the media-adventitia interface, marked by the collagen rich connective tissue layer, can be effectively demarcated using this approach B, Detailed image of the aortic wall showing bunched-up individual collagen fibrils radially arranged within elastin folds. Scale bar, 10 μm. C, Three dimensional surface reconstructions of atherosclerosis susceptible intervertebral branch points with a ring of exposed collagen immediately surrounding the ostia. Scale bar, 50 μm. D, Aortic arch branch point composed of a dense, knotted sheet of collagen. Scale bar, 50 μm.

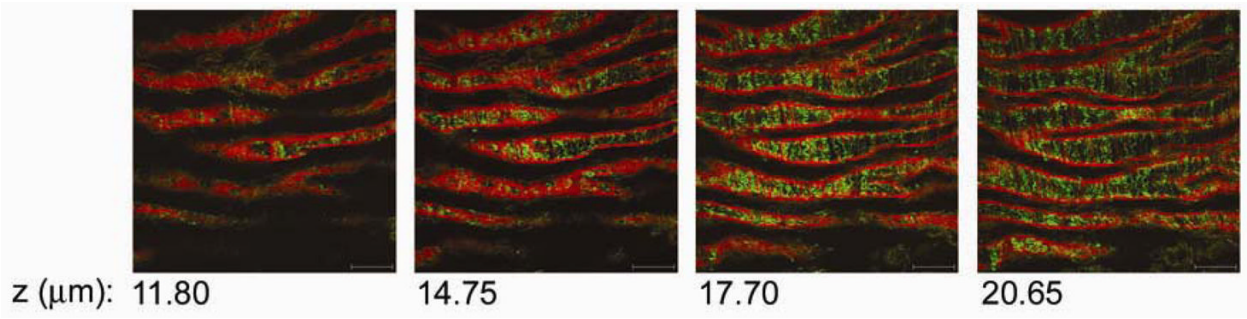

Figure 2.

Collagen and elastin microstructure of the porcine carotid artery. Selected two-photon z-series images through the porcine carotid intima, starting from the luminal surface (11.80 mm) through to the first lamellar unit. Elastin auto-fluorescence is in red and the collagen SHG is in green. A wavy sheet of elastin with circular holes throughout envelops the luminal surface of the artery. Individual, bunched-up collagen fibrils are radially arranged within the inner folds of the elastin lamellae. Scale bar, 50 μm.

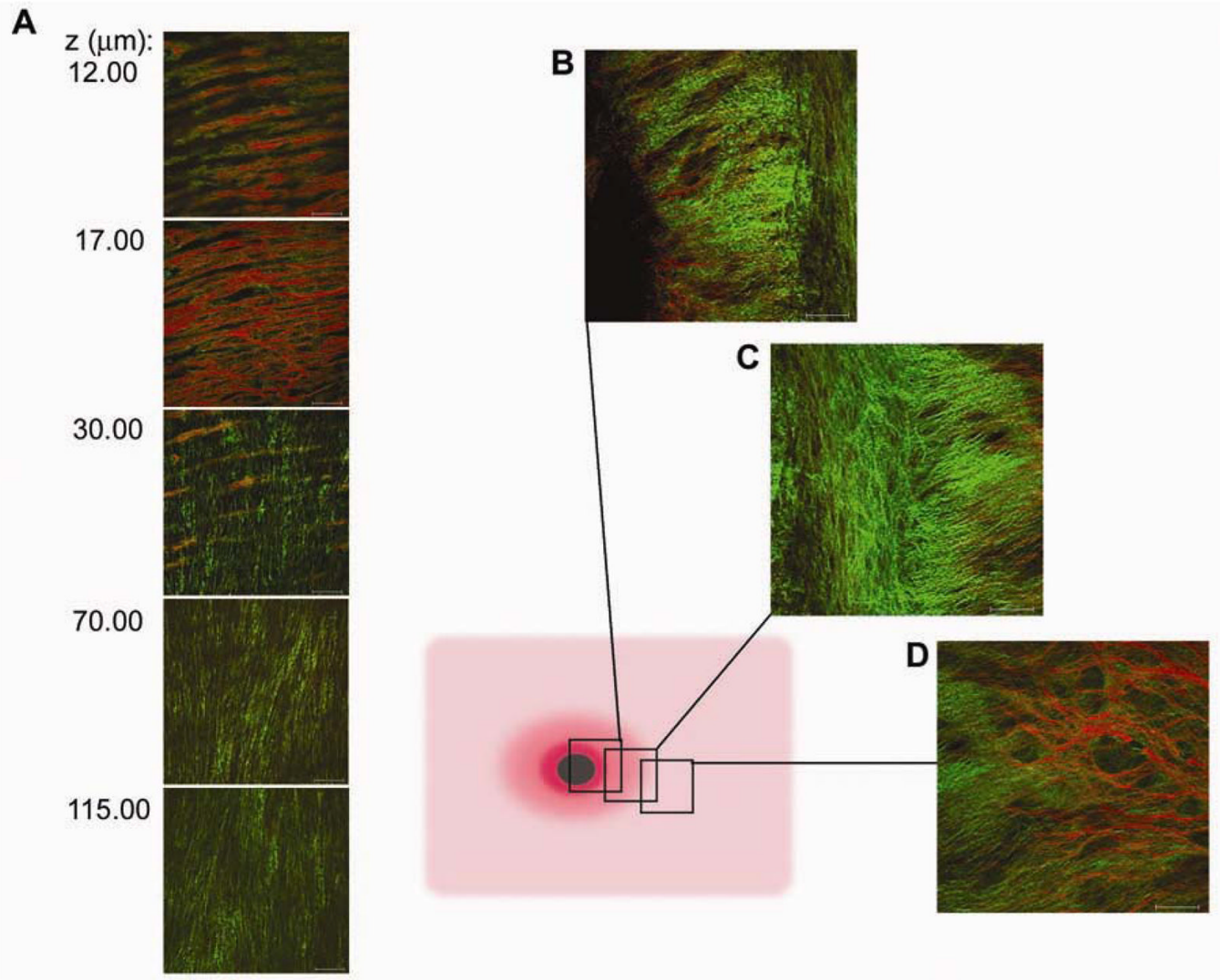

Figure 3.

Collagen and elastin microstructure of the porcine coronary artery. A, Selected two-photon z-series images from the luminal surface (12.00 μm) through to the deeper layers of the arterial media (115.00 μm). Elastin auto-fluorescence is in red and collagen SHG is in green. A net-like IEL covers the luminal surface of the coronary free wall. Diagram illustrates the areas at which images were taken along a coronary arterial branch point. B, Images were taken from the edge of the free wall. C, Densely knotted collagen structure is not covered by the IEL surrounds the ostia. D, Portion of the cut branching artery. Scale bar, 50 μm.

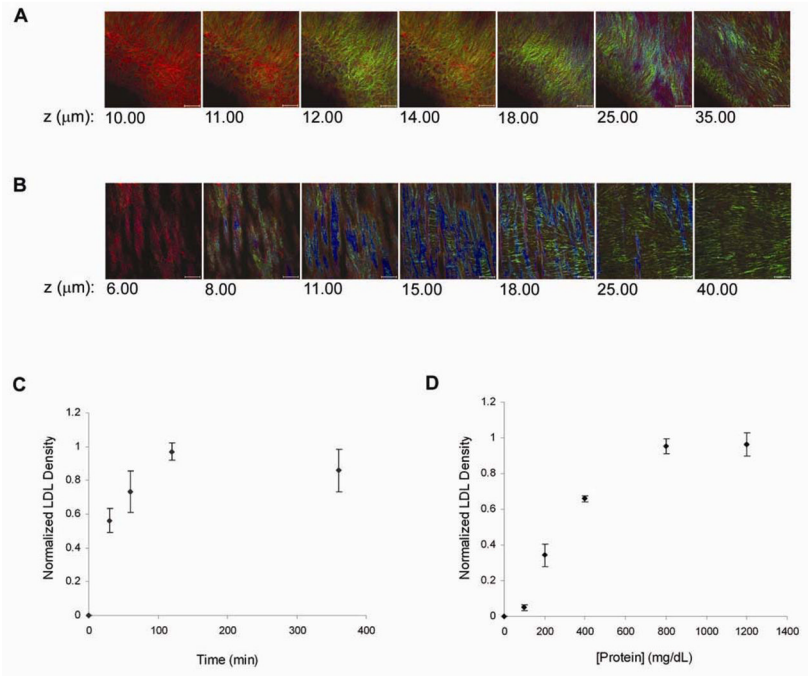

Figure 4.

LDL binding along the porcine coronary arterial wall. A, Selected z-series two-photon images of a pig coronary arterial branch point. LDL (red) bound extensively along the surface of the exposed collagen fibrils (green). Scale bar, 50 μm. B, A minimal amount of LDL (red) bound to the surface of the IEL (blue). Scale bar, 50 μm. C, Saturation curve of LDL binding to branch points at various incubation times with 2 mg/mL LDL. LDL binding reached saturation after about two hours of incubation with the artery (n = 4). D, Steady-state LDL binding studies in PBS showed a sigmoid pattern where (n = 3):

$$Y=1/(1+e^{-(x-103)/301})$$

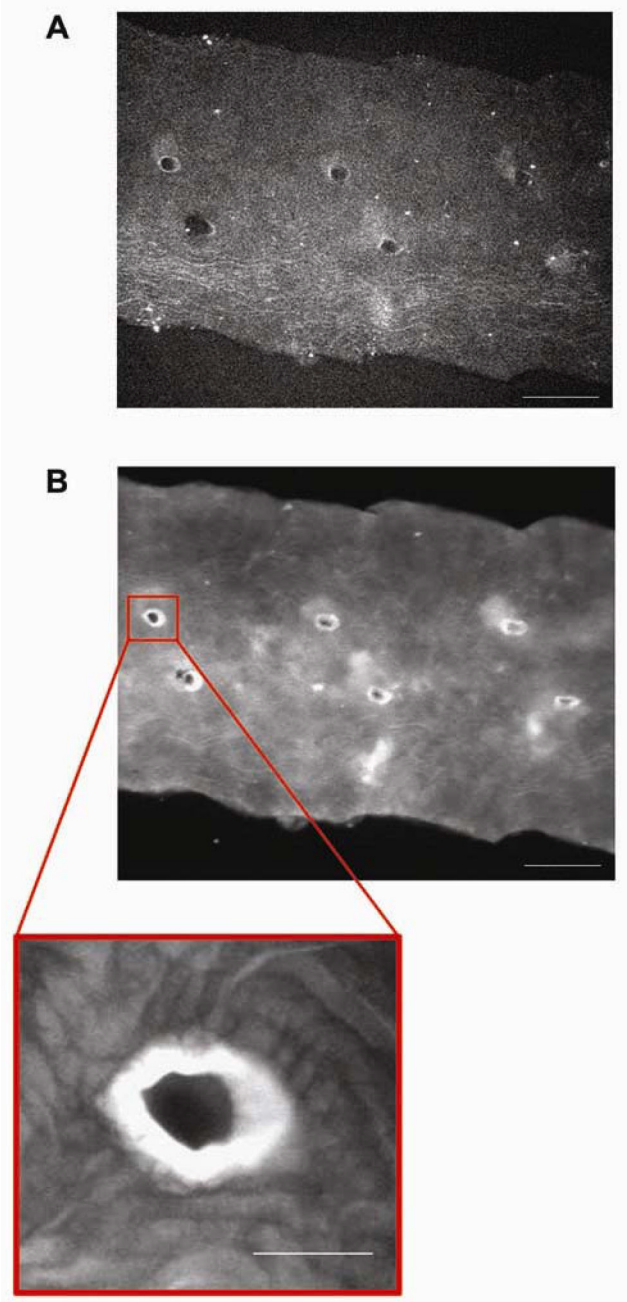

Figure 5.

LDL binding along the mouse aorta. A, Mouse aorta prior to incubation with LDL. Autofluorescence was low at 680 nm. Paired intervertebral branch points along the aortic wall became visible at a high intensity and increased exposure time (Intensity = 100%, exposure = 680 ms and gain = 165). Scale bar, 500 μm. B, Mouse aorta after incubation with LDL. LDL bound extensively to a circular region around intervertebral branch points. LDL bound lightly along the rest of the arterial wall (Intensity = 7.72%, exposure = 31 ms, Gain = 114). Scale bar, 500 μm. Zoom scale bar, 100 μm.

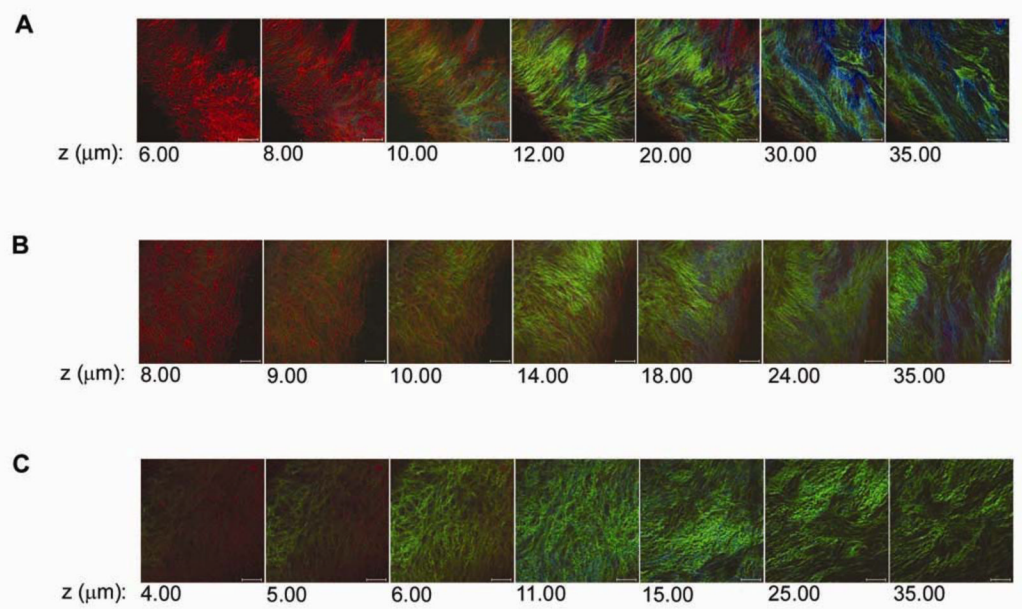

Figure 6.

LDL binding to pig coronary arterial branch points in various buffered solutions. A, LDL binding in dH_2O was very high and LDL formed insoluble complexes along the surface of the exposed collagen. B, LDL binding in normal saline was lower than that seen in dH_2O above or in bicarbonate buffer B. C, LDL in a highly anionic buffer composed of 1X PBS with 2 mM azide showed very low binding to the surface of the branch point. Scale bar, 50 μm.

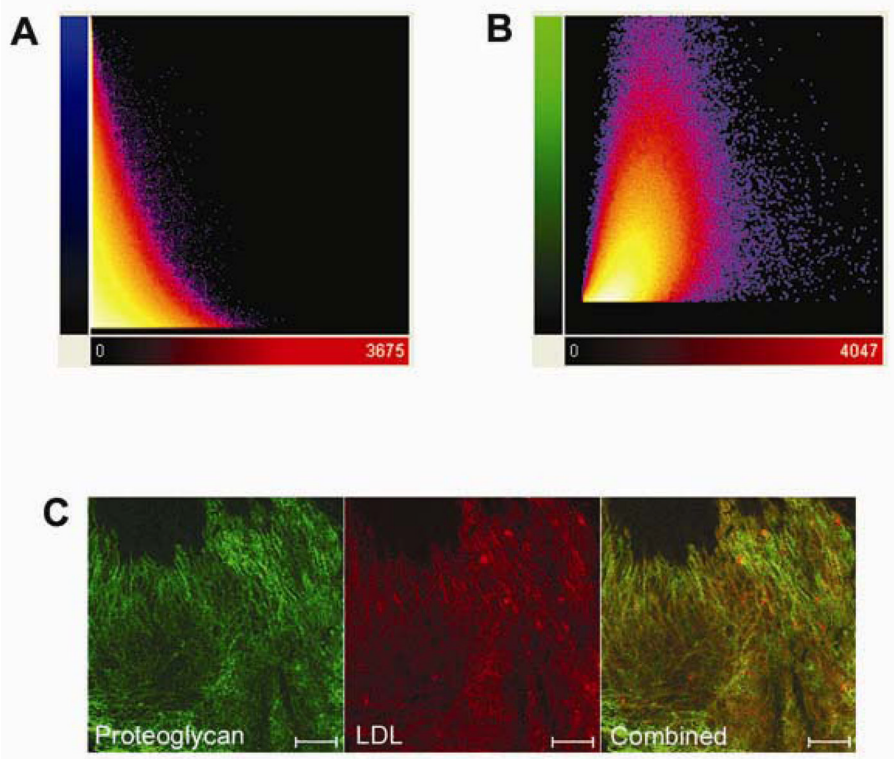

Figure 7.

Co-localization analysis of LDL binding at porcine coronary arterial branch points. A, Quantification of colocalization between collagen and LDL. Pixel codistribution was calculated for blue (collagen) and red (LDL) channels for z-series two-photon data sets. Two-dimensional histogram (fluorogram) show the distribution of pixel intensities for collagen vs. LDL with poor co-localization (n = 3). B, Quantification of co-localization between proteoglycans and LDL. Pixel co-distribution was calculated for green (proteoglycan) and red (LDL) channels. Two-dimensional histogram showed that the distribution of pixel intensities for proteoglycans vs. LDL revealing a positive spatial correlation. Pearson correlation coefficient demonstrates that there is significantly greater co-localization between LDL and proteoglycans (0.469 ± 0.030) compared with LDL and collagen (0.056 ± 0.075). (1 = perfect correlation, 0 = no correlation, and −1 = perfect inverse correlation). C, Two-photon image of LDL (red) colocalization with immunolabeled proteoglycans (green).

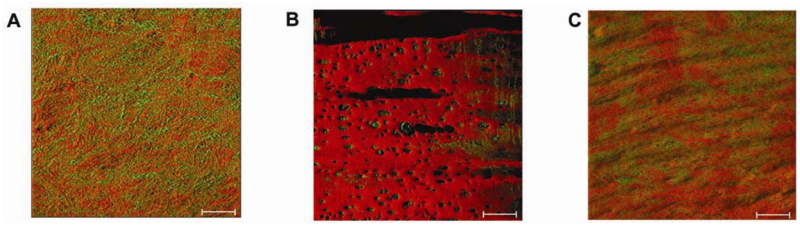

Figure 8.
Surface rendering of the porcine arterial beds. Elastin is pseudo colored red while the collagen in green. A) Aorta sample. B) Carotid sample. C) Coronary sample. Surface rendering was performed using the software resident in the Zeiss 510 imaging system.